PCCP

Accepted Manuscript

ROYAL SOCIETY OF CHEMISTRY

www.rsc.org/pccp

Physical Chemistry Chemical Physics
CREATED USING THE RSC LaTeX PCCP ARTICLE TEMPLATE – SEE www.rsc.org/electronicfiles FOR DETAILS
ARTICLE TYPE www. rsc.org/xxxxxx | XXXXXXXX

A New Magnetic Superatom: $Cr@Zn_{17}$

Alexandre Lebon,[a] Andrés Aguado,*[b] and Andrés Vega[b]

Received Xth XXXXXXXXXX 20XX, Accepted Xth XXXXXXXXX 20XX
First published on the web Xth XXXXXXXXXX 200X
DOI: 10.1039/b000000x

We demonstrate, by means of fully unconstrained density functional theory calculations, that the cluster Zn_{17} endohedrally doped with a Cr impurity can be qualified as a magnetic superalkali cluster. We explain the origin of its high stability, its low vertical ionization potential and its high total spin magnetic moment which amounts to $6\mu_B$, exactly the value of the isolated Cr atom. With the aim of exploring the possibility of designing a bistable magnetic nanoparticle, with a corresponding inter-unit exchange coupling, we also consider the assembling of two such units through different contact regions and in different magnetic configurations. Furthermore, we analyze up to which extent is the Zn shell able to preserve the electronic properties of the embedded Cr atom, both against coalescence of the two superatoms forming the magnetically bistable nanoparticle, and upon the adsorption of an O_2 molecule or even under an oversaturated O_2 atmosphere. Our results are discussed not only emphasizing the fundamental physical and chemical aspects, but also with an eye on the new prospects that those $Cr@Zn_{17}$ magnetic superalkali clusters (and others of similar kind) may open in spintronics-, molecular electronics- or biomedical-applications.

1 Introduction

Magnetism is one of the most complex and exciting phenomena in Nature, whose understanding and possible applications has motivated important efforts in the Scientific Community for a long time. Due to its collective character, magnetism involves many body effects and a subtle correlation between the structural and electronic properties. All isolated atoms with open electronic shells are magnetic as Hund's rule dictates, while in the bulk regime only few of them sustain a spin polarization and a net magnetic moment, provided that the exchange energy gain compensates the electron kinetic energy. Since the atomic and chemical environments strongly affect the magnetic properties, a large variety of magnetic behaviors can be found or even artificially created at the nanoscale. Cr is a good example of this fact. Due to its half-filled atomic electronic configuration, $3d^5\ 4s^1$, the isolated atom has a huge magnetic moment of $6\mu_B$ in its ground state, while in the bulk bcc structure, due to electron hybridization, the local spin moment is strongly quenched ($0.6\mu_B$) and the net moment is zero due to the antiparallel magnetic coupling. This strong sensitivity of the magnetic properties to the environment, typical of mid transition metal systems, is due to the high number of holes in the partially filled valence d complex. Thus, when Cr forms nanostructures, either pure or mixed with other elements, a wide range of values of the local magnetic moments can be found, as well as exotic magnetic couplings, like for instance the non-collinear arrangements developed when alloying Cr and Fe to build a topologically frustrated nanostructure[1].

For technological purposes in spintronics and molecular electronics, miniaturization is a goal and the design of magnetic grains or localized magnetic dots with stability against the environmental agents is a challenge. In order to maximize the net magnetic moment and to minimize the size, one should employ transition-metal atoms with half-filled electronic configurations, like Cr or those close to it in the Periodic Table. However, for the reasons explained above, it is quite difficult to find environments in which one of those TM atoms retains its magnetic moment or most of it. Attempts have been pursued along this line by several groups. Robles and Khanna[2] demonstrated, by means of density functional theoretical calculations, that $Cr@Si_{12}$ is a quite stable cage cluster with the Cr atom inside but in which Si-Cr electronic hybridization leads to the quenching of the Cr magnetic moment, although joining two of those stable units by certain faces, or supporting them on a Si surface provides a way to preserve a fraction of the spin-polarization in the Cr atom, since part of the Si electrons are involved in the formation of the new Si-Si bonds, thus weakening the Cr-Si hybridization. Moments up to $2\mu_B$ were predicted[2]. Palagin and Reuter[3], using a similar theoretical approach, predicted that $M@Si_{20}$ (M=Co, Ti, V and Cr) have cage structures with quenched magnetic moments, but saturating the Si atoms with H ($M@Si_{20}H_{20}$) allows to conserve the magnetic state of the isolated metal dopants. One lesson to be learnt from these studies is that the magnetic properties of the impurity can be preserved if hybridization with the cage orbitals is somehow avoided. In fact, if that is the

[a] *Laboratoire de Magnétisme de Bretagne, Université de Bretagne Occidentale, EA, 4225, 29285 Brest Cedex, France*
[b] *Departamento de Física Teórica, Atómica y Óptica, Universidad de Valladolid, Valladolid 47071, Spain; E-mail: aguado@metodos.fam.cie.uva.es*

case, the magnetic moment of the impurity might even be enhanced if the induced magnetization on the cage atoms couple ferromagnetically with that of the impurity atom. Other examples are the endohedrally doped $Mn@Sn_{12}$ cluster experimentally investigated by Rohrmann and Schäfer[4], which has a total spin moment of $5\mu_B$. The same magnetic moment was found in $V@Na_8$ by Zhang et al.,[5] who qualified this cluster as a magnetic superatom due to its high stability associated to the particular filling of molecular orbitals with the 13 valence electrons involved in bonding. $Cr@Sr_9$ and $Mn@Sr_{10}$ have been also proposed as doped magnetic superatoms, with $4\mu_B$ and $5\mu_B$ respectively, by Chauhan and Sen.[6] Finally, pure Cs_N clusters have recently provided the first example of intrinsically magnetic superatoms, where the magnetism does not involve any doping with extrinsic magnetic impurities, but is completely due to the filling of delocalized jellium-like orbitals under the constraints of Hund's rule of maximum spin multiplicity.[7]

In the present work we show a new magnetic superatom, the endohedrally doped $Cr@Zn_{17}$ cluster. This nanoalloy has $6\mu_B$, that is exactly the same magnetic moment as that of the isolated Cr atom. This is a particularly interesting magnetic grain since the host cage is made of Zn, an element that has been widely used in protective coatings against corrosive agents. We explain the origin of the high stability of this magnetic grain, which primarily comes from the fact that the pure Zn_{17} cluster itself is very stable in the hollow cage structure that hosts the Cr dopant. We further investigate the assembling of two of these units with an eye on the possible magnetic couplings between the units, which could lead to interesting spin-dependent transport properties if such contact is placed between two electrodes. Finally, we check the evolution of the magnetism of the superatom after the adsorption of an O_2 molecule and after exposure to an over-saturated oxygen atmosphere.

Density functional theoretical calculations have been conducted to optimize the structural and electronic properties of the investigated systems. The computational details are outlined in section 2. In section 3 we present first the results for the endohedrally doped $Cr@Zn_{17}$ cluster, discussing the origin of its stability and the magnetic properties. Next we analyze the complex formed by assembling two such units, with particular focus to the possible magnetic configurations and the inter-unit exchange coupling. Finally, we address the evolution of the magnetic properties of the $Cr@Zn_{17}$ superatom after the adsorption of one or many dioxygen molecules. Our conclusions are summarized in the final section.

2 Computational Methods

We performed fully self-consistent DFT calculations using the plane-wave code VASP,[8,9] which solves the spin-polarized Kohn-Sham equations within the projector-augmented wave (PAW) approach. For the exchange and correlation potential we used the Perdew-Burke-Ernzerhof form of the generalized gradient approximation.[10] The plane wave basis set was extended up to an energy cutoff of 300 eV and we used an energy criterion of 10^{-4} eV for converging the electronic part.

Local electronic charges and magnetic moments were evaluated using Bader's method[11] which is based on partitioning the cluster into atomic volumes by locating the zero-flux surfaces of the electron density field. This method is implemented in a open source code due to the group of Henkelmann[12]. Using this method, the sum of local charges and moments recovers the total electronic charge and magnetic moment. We checked that Bader's distribution of those local quantities preserves to a large extent the relative proportions directly provided by VASP through the projection of plane waves onto spherical atomic volumes.

In the calculations, the individual clusters were placed in a cubic supercell of $20 \times 20 \times 20$ Å^3, a size large enough as to make the interaction between the cluster and its replicas in neighboring cells negligible, allowing to consider only the Γ point ($k = 0$) when integrating over the Brillouin zone. In the case of two assembled clusters we enlarged the size of the supercell along one direction to $40 \times 20 \times 20$ Å^3. After the addition of an O_2 molecule, the cubic supercell was changed to $25 \times 25 \times 25$ Å^3.

The electron localization function (ELF) was computed as well, according to the definition given by Silvi and Savin[13] and implemented in VASP. Very briefly, the ELF allows for a topological analysis of local quantum-mechanical functions aimed at quantifying the effects of the Pauli exclusion principle on the electron density distribution. It defines "localization attractor basins" that allow to distinguish between the localized or metallic character of bonds, thus offering a way to analyze the nature of chemical bonding in a material. The ELF is a dimensionless quantity. Values of the ELF close to one are indicative of the localization of an electron pair in a covalent bond or of a lone pair in the non bonding situation. Values of the ELF close to one-half or lower reflect a Pauli repulsion similar to that existing in a homogeneous electron gas; this is why low ELF values are commonly associated with electron delocalization and metallic bonding.

Initial geometries were taken from an independent previous work by our group on pure Zn_N clusters.[14] In that work, global optimization techniques were used to locate the global minimum and a set of low-lying isomers for Zn_{17}, among which the cage structure has, by far, the lowest energy. We nevertheless checked other metastable structures of the host cluster to which the Cr atom was added in different positions. For the reasons explained in the next section, the endohedral cluster formed with the Cr atom encapsulated inside the cage structure of the pure Zn_{17} cluster is, also by far, the ground state

of the nanoalloy. Structures were relaxed without any symmetry or spin constraints until interatomic forces were smaller than 0.005 eV/Å. We pushed up to 0.001 eV/Å when testing non-collinear magnetic arrangements (which never were found as solutions) or when performing a vibrational analysis (which was done only for the global minimum structures, not for metastable isomers). No imaginary frequencies were detected, implying that the identified structures are stable. In all cases different spin isomers were checked in order to ensure the location of the correct ground state.

3 Results and Discussion

3.1 Stability and Magnetic Properties of $Cr@Zn_{17}$

In our previous work,[14] we explored in detail the structural and electronic properties of pure Zn_N clusters with up to $N = 73$ atoms by means of an unbiased structural search at the DFT level. The reliability of the ground state configurations was demonstrated through a benchmark of the resulting electronic structure against photoelectron spectroscopy measurements. In the particular case of Zn_{17}, we obtained a hollow cage structure with perfect D_{5h} symmetry as the global minimum (GM). Figure 1 displays the four most stable isomers of Zn_{17}. The GM structure can be viewed as a hollow 12-atom decahedron, with five additional atoms capping its square faces, but with significant distortions explained below. In figure 1, it is displayed together with the three generators of the D_{5h} group, namely the 5-fold axis which is along the vertical z direction, the σ_h mirror plane that passes through the equator, and finally the dihedral 2-fold rotational axis that is perpendicular to the plane of the figure. There are three non equivalent Zn atoms in this cluster: the five atoms belonging to the equatorial plane are 2.94 Å away from the center of the cage; the corresponding distance for the two apical or "polar" atoms on the 5-fold symmetry axis is 3.13 Å; for the remaining ten atoms that distance is 3.00 Å. These distances imply a nearly spherical cluster shape, with a slight prolate distortion, that is the cluster is more elongated along the 5-fold axis than on the equatorial plane. Notice that a "usual" capped decahedron would possess a significantly oblate shape, because the five capping atoms would be more distant from the cluster center. However, we have found[14] that Zn clusters have a marked tendency to adopt rounded spherical shapes. Upon relaxation, the originally square faces of the decahedron expand and become elongated along the $z-$axis. At the same time, the five equatorial atoms approach the cluster center. In the end, a rounded shell of monatomic thickness containing 17 atoms is obtained.

An analysis of the size dependence of the binding energies of Zn_N clusters[14] shows a marked local maximum at $N = 17$, implying the enhanced stability (magic character) of this cluster. In fact, Zn_{17} can be classified as a doubly-magic cluster, i.e. its high stability is related to simultaneously closed geometric and electronic shells. The geometric shell closing is clear from the above description. Also, with a total of 34 valence electrons, Zn_{17} has a closed electronic shell configuration that agrees with a jellium-like superatom picture ($1S^2 1P^6 1D^{10} 1F^{14} 2S^2$, see Figure 3 and corresponding discussion below). The cluster has a wide HOMO-LUMO gap of 1.3 eV, as compared to 0.4 eV for Zn_{18}, for example. Other DFT indicators confirm the enhanced stability of its electronic structure: the ionization potential (6.01 eV) and the chemical hardness are both local maxima at $N = 17$, while the electronegativity and electron affinity are marked local minima.

Cage-like clusters such as Zn_{17} are potentially interesting systems for many technological applications, as they may be selectively doped with endohedral impurities that equip the doped cluster with a chosen physical property. In turn, a stable cage may help to protect that physical property from environmental effects. In this work, we focus on magnetic prop-

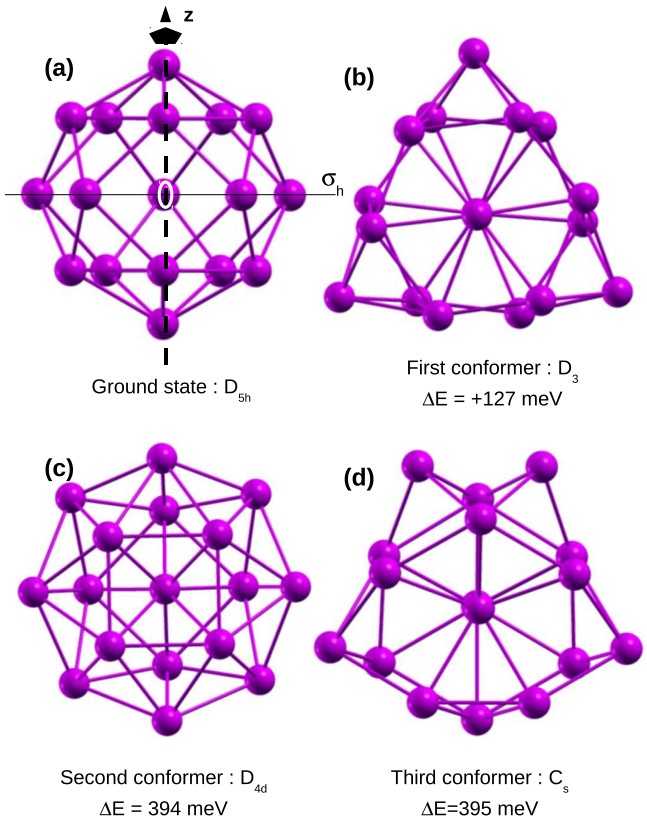

Fig. 1 Structure and symmetry of the four most stable isomers of Zn_{17}. The energy difference between each isomer and the putative global minimum is given in *meV*.

erties and choose Cr as dopant due to its high magnetic moment value of 6 μ_B. The main goal is to check in first place if the magnetic moment is preserved in the doped cluster, and if that is the case, to test in second place the degree of protection provided by the zinc cage against environmental effects. A related interest is the possibility of generating an induced magnetic moment in a non-magnetic material such as zinc.

We considered several input structures for optimization of $Cr@Zn_{17}$. Adding a Cr atom to the GM structure of Zn_{17} is the first obvious choice, and the most favorable site is the endohedral site (locating Cr outside the cage, or considering $Zn@(CrZn_{16})$ endohedral structures with an internal Zn atom, results in less stable isomers by roughly 500 *meV*). We tested several other arrangements, some of which were obtained from Zn_{18} isomers after substitution of a Zn atom by a Cr atom. These are not anymore of a hollow cage type as the Zn_{18} isomers all contain an internal Zn atom.[14] Other configurations were based on the Zn_{17} isomers with D_3, D_{4d} and C_s symmetries that are shown in Figure 1 (not cage-like), with Cr placed at different positions on the surface. In the end, the putative GM structure of $Cr@Zn_{17}$ corresponds to the endohedrally doped arrangement. We notice that the structure of the Zn_{17} host cage did not relax notoriously upon insertion of the Cr atom. In fact, the D_{5h} symmetry is preserved, the Cr impurity remains right at the cage center, and we observe only a nearly homogeneous contraction of the cage, with atomic relaxations ranging between $0.10 - 0.15$ Å. The two apical Zn atoms (those initially farther away from the central Cr atom) undergo the smallest relaxations, implying that the prolate distortion of the cage slightly increases upon doping.

The lowest energy structural excitations identified (about 50-100 meV above the GM energy) involve the displacement of the chromium impurity to an off-center endohedral position. When this happens, the zinc cage has no longer perfect D_{5h} symmetry, but is distorted with C_{2v} point group. This means that a D_{5h} cage with an off-center impurity is not found as a stable solution, and the cage rather adapts to the new position of the impurity. We notice that these C_{2v} distortions are also the lowest-energy structural excitations of pure Zn_{17}.

The spin configuration is a septet in the electronic ground state, corresponding to a total magnetic moment of $6\mu_B$, exactly the same as in the isolated Cr atom. Other inputs converged to the septet ground state during the selfconsistency cycles. Other spin isomers were checked in spin-fixed calculations. The quintet and nonet states (4 μ_B and 8 μ_B) are spin excitations at about 200 meV and 800 meV, respectively. The triplet is 1 eV less stable than the GM. The change of spin is accompanied by structural distortions, particularly important in the nonet and triplet states for which the symmetry decreases from D_{5h} to C_{2v}. We conclude that the septet is the stable configuration and thus that the magnetic moment value of the impurity is fully preserved in the nanoalloy particle.

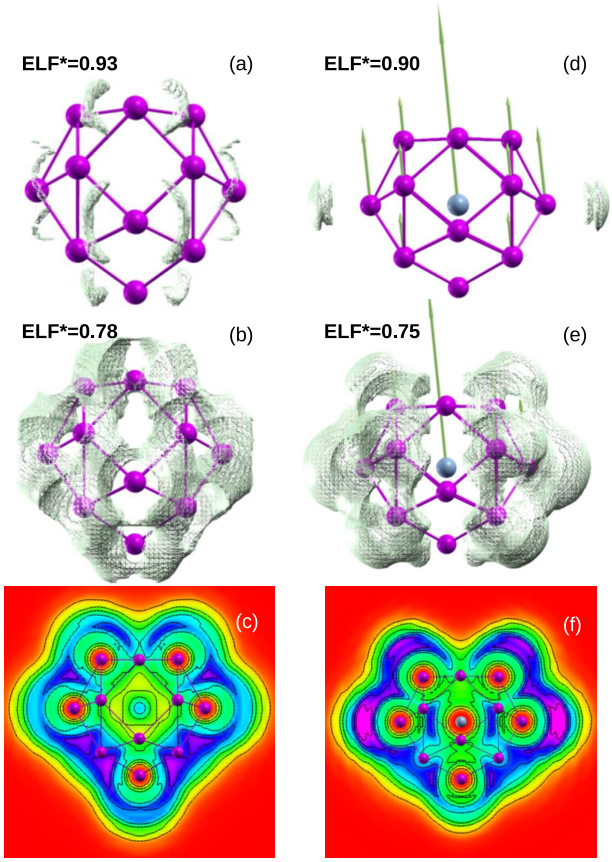

Fig. 2 Isosurface and isoline plots of the electron localization function (ELF) for Zn_{17} (left panels) and $Cr@Zn_{17}$ (right panels). The constant ELF values in the isosurface plots are given as percentages of the corresponding maximum ELF value. In the isoline plots, purple stands for the highest ELF value, and red for the lowest ELF value, with a linear interpolation between both limits according to a rainbow colour scale. Pink balls represent Zn atoms and the light blue ball represents the central Cr atom. Arrows on atoms indicate the local spin magnetic moment, which for visualization purposes is scaled by a factor of 0.2 and 2.5 for Cr and Zn, respectively.

The local magnetic moments are visualized in panels (d) and (e) of figure 2, where the doped cluster is displayed with its 5-fold axis horizontal and within the plane of the figure, and the magnetic moments are represented with arrows along the vertical direction, for the sake of clarity. Most of the magnetic moment is indeed localized on the Cr atom (about $4.8\mu_B$). The remainder ($1.2\mu_B$) is shared between the Zn atoms although not homogeneously, since two Zn atoms contribute with up to $0.15\mu_B$, few others with just $0.01\mu_B$ and most in between. The magnetic moment distribution obeys a very simple rule, the shorter the Zn-Cr distance the smaller the magnetic moment. For instance, atoms in the σ_h plane have a moment of about

0.01 μ_B whereas the two apical Zn atoms have a moment of 0.15 μ_B. The other atoms have an average magnetic moment of 0.08 μ_B. Cr-Zr magnetic couplings are parallel and thus of ferromagnetic kind, so all contributions add up. The magnetic moment induced by the impurity on the zinc cage is therefore essential for the cluster to preserve a value of $6\mu_B$ for the total moment. The non-integer value of the Cr moment indicates a Cr-Zn hybridization, however it must be weak as otherwise Cr would loose its magnetic moment[2]. Bader analysis shows that half an electron is transferred from the chromium atom to the zinc cage and shared between the 17 Zn atoms, with a maximum excess charge on a single Zn atom of 0.06 electrons. An indication of the weakness of the Cr-Zn bonding is the fact that this reduction of 0.5 electrons in the Cr atom alone would give rise to a local moment of $5.5\mu_B$, and the final Cr contribution is only slightly smaller ($4.8\mu_B$). The weak interaction between the Cr impurity and the zinc cage is in line with the results of our previous work,[14] where we demonstrated that the surface and core regions of pure Zn_N clusters are separated by an unusually long distance and so they weakly interact with each other. Thanks to such a weak Cr-Zn interaction, and the ferromagnetic-like coupling, $Cr@Zn_{17}$ retains a global magnetization of $6\mu_B$, quite a good result indeed that allows us to qualify the Cr doped Zn_{17} cluster as a stable magnetic nanoalloy.

In the following, we analyze several electronic indicators in order to better understand the nature of bonding in $Cr@Zn_{17}$. The electron localization functions (ELF) of both Zn_{17} and $Cr@Zn_{17}$ are shown in figure 2. For the pure Zn_{17} cluster, the maximum value is $ELF_M = 0.45$, a value that reflects a larger Pauli repulsion than in a homogeneous electron gas (where ELF=1/2) and thus electron delocalization. The several attractors with maximum ELF value are located on the outer region of the shell and correspond initially to three-center bonds, as they are located on top of the triangular facets and thus shared by three atoms. They are visualized in the isosurface with $ELF^* = ELF/ELF_M = 93$ % in the top left panel. The equatorial region defined by the mirror plane σ_h contains less densely packed, (100)-like, square facets where local ELF maxima are not observed. The ELF attractors merge together within each side of the cluster at a very high bifurcation value of $ELF^* \sim 90\%$. Upon further decreasing the ELF value, the isosurface encompasses the whole cluster surface, as seen in the $ELF^* = 78$ % plot. The bonding within the shell is thus of a delocalized metallic character, although with the left and right sides of the cluster maintaining a not too large connectivity. Contour isolines of the ELF are displayed in figure 2c on a plane bisecting the cluster. There we can distinguish an additional very shallow ELF attractor located at the center of the hollow cage (light blue region). This basin merges with the surface basins only at a very low bifurcation value $ELF^* = 30$ %. It emphasizes the fact the central region of the cage is not very influenced by the surface region. The bonding picture provided by the ELF analysis indicates that bonding in Zn_{17} is metallic-like, with the electron density delocalized mainly over the surface. The small size of the cage, however, produces an additional local maximum of the ELF at the center of the cage, and so the physical picture of an essentially two-dimensional rounded metal is only approximate (even if the atomic structure is two-dimensional, the electron gas has a partially three-dimensional character. This will be important when discussing the electronic shell structure below).

The ELF has been analyzed as well for the endohedrally doped $Cr@Zn_{17}$ cluster. The maximum value of ELF appears at $ELF_M = 0.28$, a smaller value than in the pure cluster. The largest ELF attractors, plotted for $ELF^* = 90$ % in figure 2d, are localized on top of the two opposite apical atoms. This is the single qualitatively different feature of the ELF as compared to Zn_{17}, and representative of a lone electron contribution to the charge density which is accumulated in a non-bonding region. Therefore, such attractors are of a non-bonding kind in the terminology of Silvi and Savin. When the ELF^* value is decreased to 75 % (figure 2e), multicenter attractors are evidenced and progressively cover the whole surface except for the equatorial plane. The qualitative picture of bonding within the shell becomes then similar to the one observed in Zn_{17}, the main difference being a small reduction in the bifurcation values of the ELF field. When the ELF^* is further decreased to 68 %, local attractors appear in between the encapsulated chromium atom and the Zn cage (some of them visible in Figure 2f), representing the weak metallic-like bonds that connect the core with the shell.

Let us turn our attention now to an analysis of the spin-polarized charge distribution. The two apical Zn atoms are the most influenced ones by Cr, as reflected in their higher magnetic moment and charge gain as compared with the rest. This is illustrated in Fig. 2d, where the magnetic moments of Zn atoms are pictorially represented by arrows; also, the charge transfer exceeds 0.05 electrons only for those two atoms. This is consistent with the lone electron density contribution identified in the ELF analysis. The global decrease induced by the dopant on the ELF values is due to the associated onset of magnetization within the whole cluster. The electrons in the outer valence shells are not any longer paired due to the spin polarization, a fact that contributes to the fall of the ELF values as compared to the paramagnetic counterpart. Despite the global fall of ELF_M, the merging of the several ELF attractor basins of the zinc cage occurs in a narrow range of ELF^* values, suggesting that Cr encapsulation does not significantly affect the metallicity of the surface.

Figure 3 shows the electron density of states (EDOS) of both pure and doped clusters. The curves have been obtained by broadening each Kohn-Sham level with a gaussian of width 0.01 eV. Local atomic contributions result from a pro-

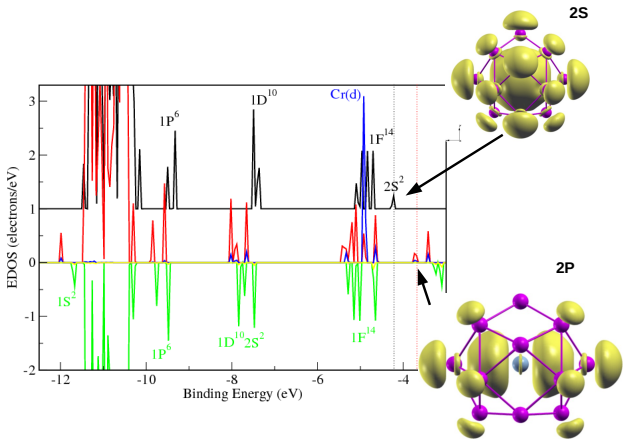

Fig. 3 The EDOS of Zn_{17} is shown with the black curve. This cluster is not spin polarized. The contribution of the 17 Zn atoms to the EDOS of $Cr@Zn_{17}$ is represented by the red (majority spin channel) and green (minority spin channel) curves, respectively. Finally, the blue and yellow lines give the corresponding contributions of the Cr impurity to the EDOS of $Cr@Zn_{17}$. Vertical dotted lines mark the position of the HOMO for the pure (black) and doped (red) clusters, respectively. The EDOS curves are normalized in such a way that their cumulative sum up to the Fermi level gives the total number of electrons. With this normalization, the minority spin contribution of the Cr atom becomes hard to appreciate visually, while the contribution from the $d-$electrons of zinc (region about -11 eV) is out of scale in the plot.

jection of the cluster wavefunction onto atom-centered spherical harmonics. Because the projections depend on the spherical volumes assigned to each atom, some interstitial charge is unavoidably lost and the sum of the atomic contributions does not fully recover the total EDOS, yet the error is small and does not alter the reliability of the level assignments. The EDOS of Zn_{17} shows a clear jellium-like shell structure, with the following filling sequence: $1S^2 1P^6 1D^{10} 1F^{14} 2S^2$ (from now on, we will employ upper-case letters to refer to delocalized superatom orbitals and lower-case letters to refer to atomic-like orbitals, following the usual convention). The assignment of levels is clear from a visual inspection of the molecular orbitals (as an example, we show in the figure an isosurface of the 2S orbital.). The 1S level is not discerned in the plot as it is hidden by the contribution of the $d-$electrons of Zn to the EDOS. The small splitting of the 1P shell is compatible with the slightly prolate shape of the cluster. For usual (three-dimensional) metallic clusters the 2S and 1D shells are close in energy and a large energy gap develops between the 2S and 1F shells, leading to an electron shell closing for $N_e = 20$ electrons. For a hollow two-dimensional metallic cage, the $S-$orbitals are strongly destabilized and one instead observes electron shell closings at 18 and 32 electrons. We indeed observe a strong destabilization of the 2S orbital, which is less stable than the 1F shell and becomes the HOMO of Zn_{17}. However, the destabilization is not so marked as to make $N_e = 32$ a magic number of electrons. This is related to the non-negligible electron density identified at the center of this small cage. In other words, Zn_{17} is just on the verge of becoming a truly two-dimensional system.

The EDOS features that we obtain for the Zn_{17} hollow cage can be rationalized in terms of a simple shell jellium model,[15] in which the nuclear density is replaced with a uniform positive charge background spread over a hollow spherical shell. In other words, a spherical hole with a given radius is pierced at the center of a typical three-dimensional spherical jellium density. The energetic ordering of the several angular momentum levels then changes as a function of the radius of the central hole. Levels with zero angular momentum ($S-$levels) are the most influenced ones as they have the largest weight at the center of the sphere on account of the absence of centrifugal repulsion effects and they are also the most compressible ones. As the radius of the hole increases, these $S-$ levels are strongly de-stabilized, i.e. pushed up in energy. The $2S-$ level soon becomes much less stable than the $1D$ level, which opens a gap at $N_e = 18$ electrons. For sufficiently large holes, even the $1F$ manifold becomes more stable than $2S$, and a gap opens at $N_e = 32$ electrons.[15] This is precisely what happens in the icosahedral Au_{32} cage (or golden fullerene)[16], with a large HOMO-LUMO gap due to its large diameter of about 0.9 nm. The diameter of the Zn_{17} cage is much smaller however (about 0.5-0.6 nm). This results to be just big enough to observe the predicted crossing of $2S$ and $1F$ levels, but without opening a large gap between them. In this case the shell jellium model predicts that a shell closing remains at $N_e = 34$ electrons, as in a filled sphere.[15] Our results are also compatible with the $2(n+1)^2$ counting rule for spherical aromaticity,[17] with $n = 3$, or with the predictions of impurity-doped jellium models,[18] in which the stabilization or de-stabilization of $S-$orbitals depends on the electronegativity of the dopant substituted at the central site of an spherical cluster. In this sense, a defect such as a vacancy can be viewed as an extreme example of an "impurity" that repels electrons from the central region.

The red and green curves show the contribution of the Zn atoms to the EDOS of $Cr@Zn_{17}$. Comparing them with the EDOS of pure Zn_{17} we can analyze the effect of the Cr impurity on the electron shell structure of the cage. A first obvious effect is that the impurity has induced a magnetization in the zinc cage. Within each spin channel, we appreciate a larger splitting of the 1P shell, which is compatible with the observed increased prolate distortion of the doped cage. All the cage orbitals become stabilized as compared to the pure cluster, reflecting the exothermicity of the doping process

($E[Zn_{17}]+E[Cr]-E[Cr@Zn_{17}]=2.28$ eV). The most important stabilization occurs for the S−orbitals due to the presence of an atom (and so of more electron density) at the center of the cage. The doped cluster is more like a filled jellium sphere rather than a hollow jellium sphere. The 1S orbital is now more stable than the d−orbitals of zinc atoms, while the energy of the 2S level is now "normal" and nearly degenerate with the energy of the 1D shell. In fact, the prolate distortion allows for the establishment of SD-hybridization within that energy window (a quadrupolar deformation allows for mixing of angular momentum states with $\Delta L=\pm 2$). Notwithstanding these changes and a slight broadening of the 1F shell, the superatom character of the zinc cage is not significantly modified by the presence of the impurity. In fact, the HOMO of the doped cluster, namely the small peak lying at about -3.6 eV, is clearly a $2P_z$ delocalized orbital, and contains one single electron. The most external part of this orbital is also visible in the ELF plot (figure 2d) as the region of highest electron localization within the cluster. Without that electron, the $[Cr@Zn_{17}]^+$ cation would become a closed shell doped superatom with a HOMO-LUMO gap of about 1 eV. Because a substantial part of the electron density associated with the $2P_z$ orbital is located outside the cage, it is easily understandable that it has quite a low binding energy. We have calculated the vertical detachment energy or VDE ($E[Cr@Zn_{17}^+]-E[Cr@Zn_{17}]$, keeping for the cation the relaxed geometry of the neutral) and obtained a value of 5.4 eV, which is quite lower than the VDE of pure Zn_{17} (6.0 eV). In fact, the VDE of $Cr@Zn_{17}$ is about the same as the ionization energy of a lithium atom, and so neutral $Cr@Zn_{17}$ can be classified as an alkali-like superatom, or "superalkali"[19–21]. We therefore expect it to be quite reactive when approaching any electronegative agent, but to keep its structural and electronic integrities in the compound as a cation. Choosing other transition metal impurities as dopants might produce other possibilities, such as closed shell superatoms with a large HOMO-LUMO gap, or halogen-like superatoms with a large electron affinity. Work is presently in progress to analyze all these exciting possibilities. We remind that in this work Cr was chosen based solely on its high magnetic moment.

The blue and yellow lines show the contribution of Cr to the EDOS of the doped cluster. The minority spin contribution is quite negligible as compared to the majority spin contribution, and so it is the Cr impurity which is responsible for the largest part of the total magnetic moment. The major contribution to the Cr EDOS is the narrow peak at around -5 eV, which is predominantly d−like as expected. The observation that almost the totality of the Cr EDOS is concentrated in a single narrow peak exemplifies the weak hybridization between the localized d−electrons of Cr and the delocalized superatom orbitals, which in turn contributes to preserve most of the magnetic moment that Cr has as an isolated atom.

In order to better understand the detailed hybridization pattern, we have first decomposed the EDOS of Cr into s, p and d angular momentum components (not shown explicitly in the figure), and observed that the contribution of $4p$−orbitals of Cr (empty orbitals in the free atom) is as significant as that of s−orbitals. The small Cr contribution to the 1S peak is completely s−like, which allows to establish a weak $s/$S hybridization. Similarly, the Cr contribution to the 1D peaks is essentially d−like, demonstrating a weak $d/$D hybridization. It is not unexpected that these are the main hybridizations observed between atom and superatom orbitals, as they are symmetry allowed even in a perfectly spherical particle for which the angular momentum is a good quantum number. Because the prolate distortion is small and so can be considered a perturbation, we do not observe appreciable s/D or d/S hybridizations. The weakness of both s/S and d/D hybridizations is explained by the absence of a resonance condition between the energies of the S and D superatom shells and the energies of the s and d atomic levels. For the same reason, the $4p$−orbitals of Cr can not appreciably hybridize with (and thus can not contribute to the spectral weight of) the 1P shell. Additionally, because the dihedral symmetry (D_{5h}) of the particle excludes the possibility of an electric dipole moment, mixing of angular momentum states with different parity is forbidden by symmetry, which explains the absence of d/F hybridization even if the $3d$ and 1F energies do satisfy a resonance condition. A weak p/F hybridization explains the small additional peaks in the Cr EDOS and also contributes to the slight broadening of the 1F superatom shell. Finally, the Cr contribution to the HOMO is also p−like, and results from p/P hybridization. This is quite understandable as the HOMO itself is a $2P_z$ superatom orbital.

In a recent work by Zhang *et al.*[5] on $V@Na_8$, the magnetism of the impurity was found to extend to the delocalized superatom orbitals of the sodium cage mainly through hybridization between the impurity and superatom orbitals. In our case, such hybridization effects are found to be very weak, so we believe that the magnetic moment of the zinc cage mostly results from a direct induction effect. After all, the information about the magnetic moment of the impurity is incorporated into the self-consistent KS potential, so the cage electrons with spin up will feel a different exchange interaction as compared to the spin down electrons. This effect of course requires a finite overlap between the orbitals of the impurity and those of the cage, but does not necessarily result in strong hybridization effects. In summary, the high magnetic moment and the electronic shell structure allow us to qualify $Cr@Zn_{17}$ as a magnetic superalkali nanoalloy.

It may be worth to state at this point what do we precisely mean when employing the "superatom" and/or "superalkali" attributes. For us, a superatom is just any multi-center molecular system that mimics the electronic behavior and shell structure of elemental atoms. In this sense, Zn_{17} is clearly a super-

atom, while $Cr@Zn_{17}$ is a doped superatom, meaning that it contains some localized *d*-levels derived from the atomic levels of the impurity and containing roughly five electrons, plus delocalized superatom-like orbitals derived from the cage orbitals and the *sp*−orbitals of chromium and containing about 35 electrons. This is the meaning that was originally assigned to the term, but as time went by, some authors added the condition that a superatom additionally has to somehow retain its structural and electronic integrity when forming compounds. This is admittedly a desirable property. However, in our opinion, adding this constraint results in an ill-defined concept, because it would not any longer be a property of the isolated cluster. In other words, a superatom may retain to some extent its identity in many compounds, but can hardly be expected to satisfy that property in arbitrary environments. In any case, that could only be asserted *after* explicitly considering the compound system. In the next sections, we will demonstrate that the $Cr@Zn_{17}$ superatom retains quite well its properties after assembling or after reacting with an oxygen molecule. However, the perfect cage structure does not persist under an oversaturated oxygen atmosphere (which may well contain more than 17 oxygen atoms, so more O atoms than Zn atoms). This is to be expected indeed, as the ionic-like Zn-O bonds are simply stronger than Zn-Zn bonds, but it does not spoil the qualification of $Cr@Zn_{17}$ as a superatom if we define that to be a property of the isolated cluster. Similarly, some authors reserve the superalkali qualification only for those superatoms with a VDE value lower than the ionization potential of the Cs atom (3.8 eV). We rather employ superalkali as a synonym of alkali-like superatom, including any multi-center system that mimics the electronic shell structure of alkali atoms.

3.2 Assembling two $Cr@Zn_{17}$ Units

Assembling two $Cr@Zn_{17}$ magnetic superatoms may be a good way to design a bistable magnetic nanoparticle, an expectation that will be confirmed in this section. Different contact regions for assembling two such units are considered. Additionally, different magnetic configurations are considered and the inter-unit exchange coupling is determined in analogy with the interlayer exchange coupling defined for magnetic multilayers employed in magnetorresistive devices[22,23]. The different magnetic states are, in principle, the antiparallel coupling between the Cr moments (AF state) and the parallel coupling (F state) which are expected to exist if the superatoms retain their identity to a large extent (no direct exchange coupling between the Cr atoms that are separated by Zn).

An important result is that no matter the contact region forming the pair, the units preserve their cage-like attribute, that is the two Cr atoms are each protected by its own Zn shell. The most stable atomic arrangement is shown in figure 4. We

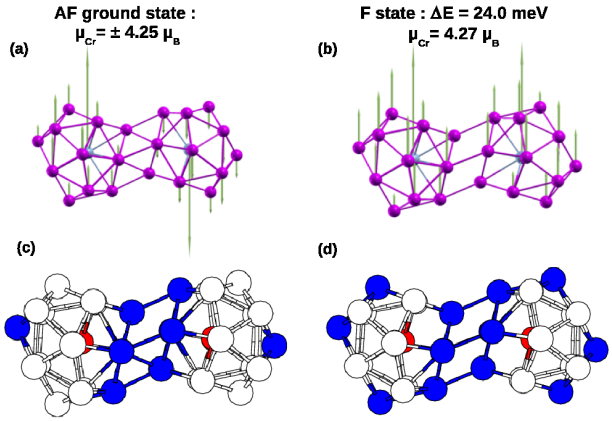

Fig. 4 Structure of the most stable $[Cr@Zn_{17}]_2$ superatom dimer, for both the AF ground state and the F excited state (a and b). Arrows on Cr and Zn atoms correspond to their local magnetic moments, which are scaled as in Fig. 2. Charge transfer on Zn atoms is displayed in panels c and d: blue balls represent atoms with a gain larger than 0.03 electrons, and white balls smaller charge transfers.

explicitly checked that there are no imaginary frequencies for this structure, implying it is a true minimum on the potential energy surface. The two superatoms connect to each other through two of their square facets, in such a way that the local atomic packing in the neck region is close to face-centered-cubic or fcc. Other arrangements have been tested, including connections between triangular and square faces, between two triangular faces, between two edges or even between two apical Zn atoms along the C_5 axis, but the most stable junction is the one formed by the fcc-like epitaxy. In fact, the stability of the different junctions increases quite steadily with the number of new Zn-Zn bonds created at the interface between the two units. The resulting point group symmetry for the superalkali dimer is C_{2h} for the F solution, while the AF state undergoes a slight distortion that lowers the precise global symmetry down to C_s. Additionally, we observe a small off-center displacement of the Cr atom towards the junction. Despite this slight distortion and the associated elastic energy cost, the assembling of the superatoms is an exothermic process and the formation energy $(2E[Cr@Zn_{17}] - E[Cr@Zn_{17}]_2)$ amounts to 2.53 eV. Overall, the most stable magnetic configuration corresponds to the AF state. The energy difference between AF and F states is 24.0 meV, which corresponds to the inter-unit exchange coupling. The total magnetic moment in the F state is $12\mu_B$, so each unit preserves a magnetic moment of $6\mu_B$, the same as for the isolated superatom.

The subtle correlation between the structure and magnetic state can be explored by performing additional single-point

calculations with fixed atomic positions. The energy cost for the vertical transition from the antiparallel ground state to the parallel state is 61 *meV* (that is the cost of one Cr spin flip keeping fixed the geometry of the AF minimum), but the resulting total spin moment is found to be 10 μ_B instead of 12 μ_B. Local relaxation of that structure lowers the energy difference by 37 *meV* and increases the total spin moment up to its optimal F value of 12 μ_B. This analysis demonstrates the necessity of considering all degrees of freedom (structural and electronic) for accurately determining the ground and excited states. A more detailed analysis of the AF→F structural relaxation reveals that the Cr-Cr distance changes by no more than 0.01 Å (from 6.40 to 6.41 Å) and that it is the environment of Zn atoms that undergoes the largest displacements, especially those Zn atoms not participating in the contact (which experience displacements of up to 0.20 Å). The Zn shell encapsulating each Cr atom is thus structurally stable but presents some flexibility. In the magnetic relaxation process, the Zn atoms displacements are an important ingredient that ultimately drives the completion of the AF→F transition.

As a general trend, the Zn atoms in each superatom unit tend to couple ferromagnetically with the Cr atom inside that unit, and thus tend to be ferromagnetically coupled also to other Zn atoms in the same unit. Representative values of the local magnetic moments on the zinc atoms are pictorially represented in the upper panels of Fig. 4. For the zinc atoms that belong to the junction, magnetic dipole values range between 0.01 and 0.07 μ_B in the AF state, and between 0.01 and 0.11 μ_B in the F state. The Zn atoms that do not participate in the contact exhibit larger moments (0.07-0.11 μ_B in the AF state and 0.08-0.14 μ_B in F). This is obviously related to their smaller coordination. Since the Cr atoms are separated by part of the surrounding Zn atoms and two magnetic states exist, one can not exclude the possibility of a non-collinear magnetic arrangement (more stable than both AF and F) in which a domain wall develops at the contact. We tested this possibility and found that different non-collinear inputs converged either to the AF or the F states. Therefore, we can qualify our superalkali dimer as a bistable magnetic system.

Concerning the charge transfer, the two lower panels of Fig. 4 highlight the regions of charge excess. Blue colour is used to represent those Zn atoms with a larger gain of electronic charge. The maximum charge transfer is found at the junction, although some charge is also tranferred to distant zinc atoms. Thus, the charge excess is more pronounced for the Zn atoms forming the contact than for the rest whose charge is quite similar to that in the isolated superatom. This feature, which is obtained both for the AF and the F states, shows that there is an accumulation of electron density in the junction region, and so is consistent with a simple bonding molecular orbital picture of the bond gluing the dimer of superatoms. In the ferromagnetic solution, there is more accumulation of charge in antibonding regions (distant from the junction), which is in line with the higher stability of the AF state. The electronic charge in the Cr atom is not affected by the formation of the pair, indicative of the high degree of isolation provided by the Zn shell.

Altogether, our results point to an indirect exchange coupling between the encapsulated Cr atoms that are separated by Zn, an analog of the situation found in the magnetic multilayers used in magnetorresistive devices[22,23]. The assembling of the two units slightly reduces the local moment in the Cr atom, that nevertheless remains quite large (around 4.3 μ_B). The total spin moment in the F state is 12 μ_B, that is twice the value of each separate unit since the moments of the Zn atoms slightly increase. Thus the Zn-Cr hybridization continues to be weak although stronger than in the isolated superatom due to the formation of the contact (which lowers the symmetry related restrictions that exist in the nearly spherical isolated superatom), a slight contraction of the zinc cages upon dimerization, and the off-center displacement of the two Cr atoms towards the contact region.

Anchoring the $Cr@Zn_{17}$ units through different contact regions led to less stable conformations than the one described above, but that otherwise are also magnetically bistable. We believe it is not necessary to provide detailed explicit information about all the metastable configurations, but it is important to notice that in the first energetically low-lying atomic arrangement, the F state resulted more stable than the AF state. In this configuration, the two units are also attached through square faces, which are however arranged to produce a square antiprism in the junction region, instead of local fcc order.

The magnetic bistability of these nanoparticles can be of potential interest for technological purposes in spintronics and molecular electronics. A magnetic bistability of the same kind was found by García-Fuente *et al.* in the clusters Mo_2X_2 (X = Fe,Co,Ni), formed by two X atoms separated by a nearly non-magnetic Mo dimer[24]. These authors found that when some of those clusters form a contact between gold electrodes, the system presents spin filtering properties and magnetorresistance driven by the magnetic state of the molecular contact. Since an external magnetic field is a way to induce a change in the magnetic state of the contact, they could also act as field sensors depending on the spin-dependence of their electronic transport properties. Negulyaev *et al.* demonstrated the possibility of using also electric fields as a switching tool for magnetic states in atomic nanostructures[25], in that case for a Mn dimer supported on Ag(001) and Ni(001) which presented also magnetic bistability. Due to the superatomic character of $Cr@Zn_{17}$, we expect it to preserve its identity to a large extent upon deposition on certain substrates, possibly as a cation due to its superalkali nature (if this is the case, the positive charge on the supported particles might help to alleviate coalescence problems, which might be useful to deposit ordered arrays of

superatoms on a substrate with nanolithography techniques). All the above possibilities deserve to be investigated in the future, both theoretically and experimentally, for the $Cr@Zn_{17}$ nanoparticles discovered in the present work and/or with other transition metal dopants.

3.3 Adsorption of O_2 on $Cr@Zn_{17}$

We have considered the adsorption of an O_2 molecule on different sites of $Cr@Zn_{17}$, with the aim of quantifying up to which extent is the Zn shell able to preserve the electronic properties of the embedded Cr atom. We remind the reader that Zn is often used in protective coatings against several environmental conditions, and that Cr is very sensitive to the atomic and chemical environment, up to the point of easily loosing its magnetic moment as described in the introduction. Because $Cr@Zn_{17}$ is a superalkali, we expect that it transfers its loosely bound electron and thus react strongly with O_2, so this is really a stringent test of the ability of the Zn cage of preserving the magnetic properties of the impurity. Four different adsorption sites were chosen as initial geometries (see the upper left corner in Figure 5): three of them correspond to placing the O_2 molecule in an atop position and with parallel orientation over each of the three Zn atoms which are not equivalent by symmetry; in the fourth one, the O_2 molecule is placed on top of one of the equatorial square facets. A search for the ground state spin configuration was carried out separately for each adsorption site. Although we realize that these specific choices do not exhaust all the possible adsorption sites, and that we have not explicitly considered the possibility of dissociative chemisorption, we believe they are enough to obtain useful preliminary insights about the response of the chromium atom. A more exhaustive study of the reactivity of $Cr@Zn_{17}$ is currently in progress and will be shown in a separate publication.

Relaxed geometries are shown in Fig. 5. The putative ground state configuration has a total magnetic moment of $4\mu_B$. The calculated molecular adsorption energy is 2.81 eV, indicative of a strong interaction between the cluster and the adsorbate. The first excited isomer is located 112 *meV* above the energy of the global minimum, and corresponds to a pure spin excitation. Although the adsorption of an O_2 molecule induces a $2\mu_B$ reduction in the total magnetic moment, the Cr atom looses less than $1\mu_B$, and so still preserves more than $4\mu_B$, which is similar to the value obtained in the superalkali dimer and more than the spin moment of most transition-metal atoms.

Let us analyze in more detail now the structural and electronic changes undergone upon O_2 adsorption. The Zn atoms that form bonds with oxygen are subjected to the largest relaxations, as expected. After the adsorption process, the O-O bond length becomes $d_{O-O} = 1.53$ Å, so it elongates by

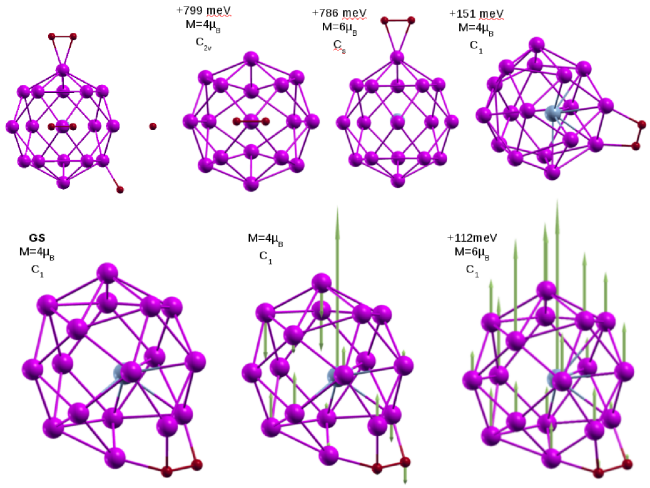

Fig. 5 Structure of $Cr@Zn_{17}$ with an adsorbed O_2 molecule. The top left panel shows the four input geometries, for which $2\mu_B$,$4\mu_B$ and $6\mu_B$ total magnetic moments were tested. The next top panels present the geometries and point group symmetries of several conformers, while the left bottom panel displays the putative ground state geometry. The last two bottom panels show the magnetic moment on Cr and Zn atoms for the two most stable spin isomers of the global minimum geometry (the scaling factors are the same as in figure 2).

0.3 Å as compared to the molecule *in vacuo*. The Cr atom experiences a slight off-center displacement towards the O_2 molecule. Before O_2 uptake by $Cr@Zn_{17}$, the average Zn-Cr distance amounts to 3.00 Å with a standard deviation of 0.05 Å . This average separation rises to 3.05 Å after O_2 uptake, in accord with an expansion of the cluster. In addition the standard deviation of the Zn-Cr separation reaches a value of 0.29 Å , underlining a slight shape distortion (elongation) induced in the adsorption process. For the global minimum with $4\mu_B$ this elongation is slightly more marked than for the $6\mu_B$ isomer.

In the lower panels of Fig. 5 we illustrate the local magnetic moments distribution for the two spin isomers. The electronic charge lost by the Cr atom amounts to 0.47 electrons, that is essentially the same as in the bare $Cr@Zn_{17}$. This is a strong indication that the Zn coating preserves the properties of the central region even after oxidation. In fact, most of the adsorbate-induced charge transfer occurs within the Zn shell, especially in the vicinity of the oxygen atoms. The charge gained by the adsorbate is about 0.6 electrons per oxygen atom, so the elongated adsorbed oxygen molecule is in a superoxo (O_2^-) state. This is in line with the monovalent (superalkali) nature of the $Cr@Zn_{17}$ unit. In fact, we notice that on most metallic surfaces O_2 rather prefers to adsorb in a peroxo (O_2^{2-}) state, which is an intermediate stable state before

dissociation into two O^{2-} anions.[26] That we observe a superoxo state is an explicit demonstration of the high stability of the closed-shell $[Cr@Zn_{17}]^+$ cation. The magnetic moment on the Cr atom decreases with respect to the superatom by approximately 0.8 μ_B in the global minimum with $4\mu_B$ and by 0.5 μ_B in the $6\mu_B$ spin isomer. This decrease of the local magnetic moment of chromium explains only a part of the $2\mu_B$ drop in the total moment. The more important contribution is the anti-parallel coupling developed between the Zn atoms (see Fig. 5), contrary to what is observed in both the $6\mu_B$ isomer and the isolated $Cr@Zn_{17}$ superatom.

Finally, we have also performed calculations with a large number of O_2 molecules in order to study the response of the superatom to an oxygen-oversaturated environment. In these preliminary calculations, we have simply attached ten O_2 molecules at initial positions which are equivalent by symmetry to the initial position that led to the largest adsorption energy for a single O_2 molecule. Such an initial structure is shown in Figure 6a. We emphasize that by no means do we expect this initial structure to result into anything near the true GM structure of the $Cr@Zn_{17}[O_2]_{10}$ system. A more detailed and systematic study of $Cr@Zn_{17}[O_2]_m$ systems, in which oxygen molecules are sequentially attached to the cage and relaxed, is now in progress. In fact, it is quite probable that the cohesive energy as a function of m presents a maximum at some $m < 10$ value. Our only goal here is to probe the cage ability for preserving the magnetic properties of the endohedral impurity even under extreme environmental conditions, and this simple calculation may already provide some clues.

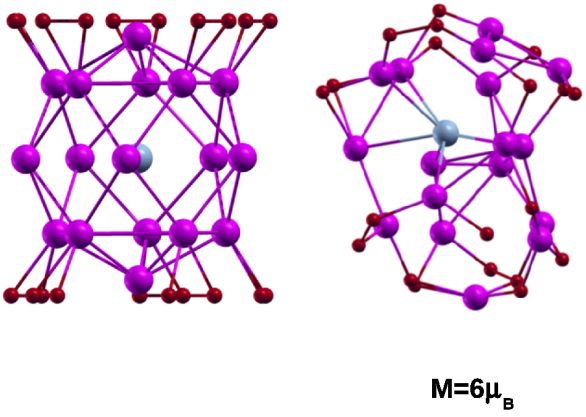

Fig. 6 Structure of $Cr@Zn_{17}$ with 10 adsorbed O_2 molecules. The left panel shows the initial position of O_2 molecules, and the right panel the relaxed geometry.

After a relaxation of forces, we found that the cluster preserves a high magnetic moment despite the attack of the many O_2 molecules. In fact, we tested $4\mu_B$, $6\mu_B$ and $8\mu_B$ isomers, and the relaxation process produced an energy minimum for the $6\mu_B$ isomer. In this isomer (see fig. 6b), Zn atoms maintain a spatial arrangement around the Cr atom and protect the open shell element from forming bonds with the external oxygen atoms. The high symmetry of the input structure becomes progressively destroyed during the relaxation process, and in the relaxed structure (amorphous, with C_1 symmetry) the original cage can hardly be recognized. Nevertheless, the first atomic coordination layer about Cr is composed only by Zn atoms, and moreover the Cr-Zn bonds contract in the process: the relaxed Cr-Zn distances range between 2.60 and 2.80 Å (this should be compared to an average $d_{Zn-Cr} = 3.00$ Å in the isolated superatom).

What is then the effect of adding large amounts of a corrosive agent such as oxygen? Not only does it not destroy the magnetism, but it rather strengthens it due to a stronger Zn-Cr bonding! The high value of the obtained magnetic moment is very promising especially when compared to previous work[4]. Further studies, including the progressive addition of corrosion agents such as dioxygen, *CO*, or water molecules are now in progress and will be reported elsewhere. The study of such corrosion agents is of prime importance in order to assess whether the cluster might be useful as a functional magnetic nanoparticle for biomedical applications. At present, only Co nanoparticles or iron oxide nanoparticles are used for magnetic resonance imaging (MRI). These particles, with diameters about 3-4 nm, could be easily excreted from the body. With its smaller size (less than 2 nm) and a high magnetic moment, the $Cr@Zn_{17}$ superatom might be a perfect candidate for medical applications such as MRI[27].

4 Conclusions

Fully self-consistent DFT calculations, using the plane-wave code VASP within the projector-augmented wave approach and the Perdew-Burke-Ernzerhof form of the generalized gradient approximation, led us to find a new magnetic superatom: the endohedrally doped $Cr@Zn_{17}$ cluster. Its high stability relies primarily on the doubly-magic character of the bare Zn_{17} cluster which has a D_{5h} hollow cage structure and simultaneous closing of geometric and electronic shells. Embedding Cr inside the Zn cage results in an exothermic process in which the superatom character of the zinc cage is not significantly modified, but it leads to a spin-polarized electronic configuration of $Cr@Zn_{17}$ with a high total moment of $6\mu_B$, most of which ($4.8\mu_B$) localized on the Cr atom. The weak Cr-Zn interaction together with the magnetic moment induced by the impurity on the zinc cage and the parallel magnetic coupling between Cr and Zn are essential features for preserving such total moment similar to the one of the isolated Cr atom.

The value obtained for the vertical detachment energy of $Cr@Zn_{17}$ (5.4 eV) is quite lower than that of pure Zn_{17} (6.0 eV) and about the same as the ionization energy of a lithium atom. Therefore, our $Cr@Zn_{17}$ can be also classified as an alkali-like superatom, or "superalkali", due to which we expect it to be quite reactive when approaching any electronegative agent, but to keep its structural and electronic integrities in the compound as a cation. Therefore, we expect it to preserve its identity to a large extent upon deposition on certain substrates, possibly as a cation due to its superalkali nature in which case the positive charge on the supported particles might help to alleviate coalescence problems and facilitate the deposition of ordered arrays of superatoms on a substrate with nanolithography techniques. Choosing other transition metal impurities as dopants might produce other possibilities, such as closed shell superatoms with a large HOMO-LUMO gap, or halogen-like superatoms with a large electron affinity. Work is presently in progress to analyze all these exciting possibilities.

We have shown that assembling two $Cr@Zn_{17}$ units (exothermic process also) is a good way to design a bistable magnetic nanoparticle, that is, with both parallel and antiparallel magnetic solutions no matter the contact region forming the pair. The inter-unit exchange coupling amounts to 24.0 meV in the most stable structural junction. This points to an indirect exchange coupling between the encapsulated Cr atoms (which only loose $0.5\mu_B$) that are separated by Zn, a molecular analog of the situation found in the magnetic multilayers used in magnetorresistive devices. The magnetic bistability of these nanoparticles can be of potential interest for technological purposes in spintronics and molecular electronics.

Finally, we have shown that the encapsulated Cr atom preserves a high magnetic moment despite the attack of one O_2 molecule or even under an oversaturated O_2 atmosphere. Zn atoms maintain a spatial arrangement around the Cr atom and protect the open shell element from forming bonds with the external oxygen atoms. Further studies, including the progressive addition of corrosion agents such as dioxygen, *CO*, or water molecules are now in progress and will be reported elsewhere. The study of such corrosion agents is of prime importance in order to assess whether the cluster might be useful as a functional magnetic nanoparticle for biomedical applications. With its smaller size (less than 2 nm) and a high magnetic moment, the $Cr@Zn_{17}$ superatom might be a perfect candidate for medical applications such as MRI.

We acknowledge the support of the Spanish Ministry of Science and Innovation and the European Regional Development Fund (grant no. FIS2011-22957). A.V. acknowledges the financial support and kind hospitality from the University of Brest (UBO), France. Facilities provided by the Pole de Calcul Intensif pour la Mer, CAPARMOR (Brest) are also acknowledged.

References

1 R. Robles, E. M. nez, D. Stoeffler and A. Vega, *Phys. Rev. B*, 2003, **68**, 094413.
2 R. Robles and S. N. Khanna, *Phys. Rev. B*, 2009, **80**, 115414.
3 D. Palagin and K. Reuter, *Phys. Rev. B*, 2012, **86**, 045416.
4 U. Rohrmann and R. Schäfer, *Phys. Rev. Lett.*, 2013, **111**, 133401.
5 X. Zhang, Y. Wang, H. Wang, A. Lim, G. Gantefoer, K. H. Bowen, J. Ulises-Reveles and S. N. Khanna, *J. Am. Chem. Soc.*, 2013, **135**, 4856.
6 V. Chauhan and P. Sen, *Chem. Phys.*, 2013, **417**, 37.
7 A. Aguado, *J. Phys. Chem. C*, 2012, **116**, 6841.
8 G. Kresse and J. Hafner, *Phys. Rev. B*, 1993, **47**, R558.
9 G. Kresse and J. Furthmüller, *Phys. Rev. B*, 1996, **54**, 11169.
10 J. P. Perdew, K. Burke and M. Ernzerhof, *Phys. Rev. Lett.*, 1996, **77**, 3865.
11 *Atoms in Molecules. A Quantum Theory*, ed. R. F. W. Bader, Clarendon, Oxford, 1990.
12 G. Henkelmann, A. Arnaldsson and H. Jónsson, *Comput. Mater. Sci.*, 2006, **36**, 354.
13 B. Silvi and A. Savin, *Nature*, 1994, **371**, 683.
14 A. Aguado, A. Vega, A. Lebon and B. von Issendorff, *Unpublished results*.
15 W.-J. Yin, X. Gu and X.-G. Gong, *Solid State Commun.*, 2008, **147**, 323–326.
16 M. P. Johansson, D. Sundholm and J. Vaara, *Angew. Chem. Int. Ed.*, 2004, **43**, 2678–2681.
17 A. Hirsch, Z. Chen and H. Jiao, *Angew. Chem. Int. Ed.*, 2000, **39**, 3915.
18 E. Janssens, S. Neukermans and P. Lievens, *Curr. Opin. Solid State Mater. Sci.*, 2004, **8**, 185–193.
19 N. Hou, D. Wu, Y. Li and Z.-R. Li, *J. Am. Chem. Soc.*, 2014, **136**, 2921.
20 S. Giri, S. Behera and P. Jena, *J. Phys. Chem. A*, 2014, **118**, 638.
21 W. Sun, Y. Li, D. Wu and Z. Li, *J. Phys. Chem. C*, 2013, **117**, 24618.
22 M. N. Baibich, J. M. Broto, A. Fert, F. N. V. Dau, F. Petroff, P. Etienne, G. Greuzet, A. Friedrich and J. Chazelas, *Phys. Rev. Lett.*, 1998, **81**, 2472.
23 G. Binasch, P. Grünberg, F. Saurenbach and W. Zinn, *Phys. Rev. B*, 1989, **39**, 4828.
24 A. G. a Fuente, V. M. G. a Súarez, J. Ferrer and A. Vega, *Phys. Rev. B*, 2012, **85**, 224433.
25 N. N. Negulyaev, V. S. Stepanyuk, W. Hergert and J. Kirschner, *Phys. Rev. Lett.*, 2011, **106**, 037202.
26 M. Neumaier, M. Olzmann, B. Kiran, K. H. Bowen, B. Eichhorn, S. T. Stokes, A. Buonaugurio, R. Burgert and H. Schnöckel, *J. Am. Chem. Soc.*, 2014, **136**, 3607.
27 Q. A. Pankhurst, N. K. T. Thanh, S. K. Jones and J. Dobson, *J. Phys. D: Appl. Phys.*, 2009, **42**, 224001.